

Research Article

OPTIMIZATION OF AIR CHANNEL GEOMETRY ON TROMBE WALL FOR TRANSMITTING EXCESSIVE HEAT

Pouyan Mohseni Behbahani¹, Reza Bahoosh Kazerouni² and Hassan Davar³

¹Department of Mechanical Engineering, Deylam Branch, Islamic Azad University, Khuzestan, Iran

²Department of Mechanical Engineering, Shahid Chamran University of Ahvaz, Ahvaz, Iran

³Department of Mechanical Engineering, Ramhormoz Branch, Islamic Azad University, Khuzestan, Iran

*Author for Correspondence

ABSTRACT

Free heat convection was simulated in a room affected three-dimensionally by Trombe wall for laminar and turbulent flows. Direct solar radiation was modeled using solar positioning vector and radiation parameters. Solar ray tracing algorithm was modeled using solar positioning vector and radiation parameters. The results were compared with those of experimental models to choose the appropriate turbulence model. The results indicate that the low Reynolds shear stress model was a superior model as a turbulence model. The optimized geometry of Trombe wall was chosen in a way to transmit optimum heat in a range of Rayleigh values from 10^7 to 10^{10} with the help of Nusselt values. The results revealed that the optimized geometrical parameters including the distance of the heat wall from the glass, wall thickness and upper and lower channels are decreased by Rayleigh number. An investigation into the effects of sharp corners of air channels in heat transmittance displayed that by removing such sharp corners the heat transmittance and the room temperature can be substantially increased.

Keywords: Optimization, Trombe Wall, Free Convection, Building Heating, Numerical Simulation

INTRODUCTION

The current global energy crisis has changed the optimum consumption of energy resources and their preservation into a vital task. There are several possibilities for saving energy. Heating, cooling and air ventilation greatly contribute to energy consumption. Much of energy demands in buildings and facilities can be met using renewable energies including solar energy. One of the heating methods is indirect absorption by Trombe wall. Trombe wall is a south-facing thick wall covered by a slightly distanced glass surface and a channel in between. The outer surface is dark to absorb solar energy.

There are two types of Trombe walls: Trombe walls with air circulation and Trombe walls without air circulation. The present paper concerns Trombe walls with airflow circulation. Several studies have been carried out regarding Trombe walls. Akbari and Borges (1979) suggested terms for flow speed through Trombe wall by solving a series of Navier-Stokes equations. Chen and Zhung (2006) showed in an empirical study that the natural synergy in the channel is somehow complicated because a laminar flow is turned to a turbulent flow covering half of the height of the thick wall. Gala and Sajda (2006) used $k-\varepsilon$ method to simulate free movement flow in a room and examined the influence of construction material on the thermal wall. Smole and Thomas (1993) stated that the synergized transfer of heat through Trombe wall depends on the performance of the lower vents.

Fedorov and Viskanta (1997) used Low Re $k-\varepsilon$ to calculate induction flow and heat transfer through an asymmetrical warmed vertical channel. They reported that the disturbance in channel entrance affects the point where planar flow is turned into turbulent flow. Peng and Davison (1999) applied upset model $k-\varepsilon$ to describe disturbance resulting from the natural advection in the hole.

Kaiser *et al.*, (2004) stated that the sample algorithmic functions of wall, as compared to the imposed boundary layer, are not suitable for numerical computations. Hence they used upset model Low Re $k-\varepsilon$ and general phonetic code based on infinite volume method.

A review of the literature shows that no precise three-dimensional simulation has been conducted on the influence of variations in air-passing channels and the role of Rayleigh number on heat transfer. The present paper applied numerical solution to examine induced flows resulting from natural advection in

Research Article

channels of Trombe wall using three-dimensional geometry and the free movement flow in a room for simulated laminar and turbulent flows. An optimized geometry was obtained for maximized heat transfer. Then, the influence of Rayleigh number on heat transfer was shown.

The main objective is the analysis of geometric parameters that depend on the induced thermal Archimedes flow between warmed walls. Although several papers have been published on the Archimedes flows indicating air heaters such as Trombe wall and solar chimney, a few have been concerned with turbulent flows. The extant paper mainly focuses on transferring and turbulent flows.

Governing Equations

In the analysis of a laminar or turbulent fluid flow, one should use continuity, momentum and energy equations which are the most inclusive equations for viscous currents. The solution of Navier-Stokes equations by applying the existing boundary conditions results into the appropriate form of the fluid flow pattern and heat transfer. All the existing parameters of laminar flow equations can be divided into two general categories including mean and varying equations. The continuity to differential form equation is given as follows:

$$\frac{\partial}{\partial x_i}(\rho u_i) = 0 \tag{1}$$

The momentum equation for turbulent flows is proposed as follows:

$$\rho \left(\bar{u}_j \frac{\partial \bar{u}_i}{\partial x_j} \right) = \bar{B}_i - \frac{\partial \bar{p}}{\partial x_i} + \left(\mu \frac{\partial \bar{u}_i}{\partial x_j} - \overline{\rho u'_i u'_j} \right) \tag{2}$$

The only difference between the resulted momentum equation and instantaneous quantities momentum equation is the addition of the last term on the right-hand side of the equation i.e. $(\overline{\rho u'_i u'_j})$. This term is called *Reynolds strain* and marks the difference between quite and turbulent flows equations (Versteeg and Malalasekera, 1995).

$$\frac{\partial(Tu_j)}{\partial x_j} = \frac{\partial}{\partial x_j} \left(\frac{\nu}{Pr} \frac{\partial T}{\partial x_j} - \overline{T'u_j} \right) \tag{3}$$

Simulation of Room under Study by Different Turbulent Flow Models

Since Ra=10¹⁰, it is required to use turbulent flow models in order to simulate flow free movement. Also, considering the existence of buoyancy forces, one can use *k-ε* or Reynolds strain transfer models to solve the relative equations (FLUENT 1998). Hence, Standard *k-ε* and RNG *k-ε*, and Low-Re stress-omega and Linear pressure-strain models methods were used for modeling the purpose. In order to select the appropriate turbulence model and verification of the chosen numerical solution, modeling results were compared with experimental results by Chen and Zhuang (2006).

Modeling results are presented in Table 1. Numerical modeling errors (in percent) are compared with those of experimental modeling in Table 2.

Table 1: The results of numerical models and experimental model

Model	\overline{Nu}_1	\overline{Nu}_2	$T(C^\circ)$
Experimental	149.03	112.34	18
Low-Re stress omega	160.95	123.08	21
Linear pressure Strain	162.65	126.14	22.12
RNG <i>k-ε</i>	174.23	129.38	24.02
<i>k-ε</i>	177.64	131.14	26.72

Research Article

Table 2: Percent error in the numerical models compared with empirical model

Model	\overline{Nu}_1	\overline{Nu}_2	$T(C^\circ)$
Low-Re stress omega	8	9.5	16.66
Reynolds stress Linear pressure Strain	9.1	12.36	22.88
RNG $k - \varepsilon$	16.90	15.16	33.44
$k - \varepsilon$	19.19	16.73	48.44

The main reason of proximity between results of stress-strain models and those of experimental models is that in the former, 6 transfer models are used to precisely determine the distribution of Reynolds shear stress while in two-equation $k-\varepsilon$ models with considered six Reynolds stress unknowns, one can be certain that only two stresses have been precisely determined and others are imprecise. As far as one component of Reynolds stress tensor is concerned, eddy-viscosity models for boundary layer flows are suitable. In such flows, eddy-viscosity model is an expression of dominating Reynolds stress component. However, the flow defies matching this simple assumption is no longer valid in eddy-viscosity models. Hence the validity of such models is questionable. By comparing the obtained numerical results with those of experimental models it was observed that the Low-Re stress-omega model was used as the suitable turbulence model.

$$\frac{D}{Dt}(\overline{u'_i u'_j}) = \frac{\partial(d_{ijk})}{\partial x_k} + P_{ij} + G_{ij} + \phi_{ij} + \varepsilon_{ij} \quad (4)$$

Where turbulence movement due to mean flow is:

$$\frac{D}{Dt}(\overline{u'_i u'_j}) = u_k \frac{\partial(\overline{u'_i u'_j})}{\partial x_k} \quad (5)$$

Turbulence development due to mean bending is:

$$P_{ij} = - \left[(\overline{u'_i u'_k}) \frac{\partial(\overline{u'_j})}{\partial x_k} + (\overline{u'_j u'_k}) \frac{\partial(\overline{u'_i})}{\partial x_k} \right] \quad (6)$$

Turbulence development due to volume force is:

$$G_{ij} = (\overline{u'_i f'_j} + \overline{u'_j f'_i}) \quad (7)$$

Correlation between pressure and turbulent bending is:

$$\phi_{ij} = \frac{P'}{\rho} \left(\frac{\partial u'_i}{\partial x_j} + \frac{\partial u'_j}{\partial x_i} \right) = \frac{2P'}{\rho} S'_{ij} \quad (8)$$

Turbulence disappearance is obtained by:

$$\varepsilon_{ij} = 2\nu \frac{\partial u'_i}{x_k} \frac{\partial u'_j}{x_k} \quad (9)$$

Research Article

Also, turbulence diffusion is obtained as follows:

$$d_{ijk} = -\frac{P}{\rho} (u'_i \delta_{jk} + u'_j \delta_{ik}) + \nu \frac{\partial (\overline{u'_i u'_j})}{\partial x_k} - \overline{u'_i u'_j u'_k} \quad (10)$$

Since the corresponding term of turbulence dynamic energy is $(1/2)k = \overline{u'_i u'_j}$, one can infer from Eq. (7) that by switching j and k indices and dividing the obtained equations into two, the turbulence dynamic energy transmittance can be obtained as follows:

$$\frac{Dk}{Dt} = \frac{\partial d_i^{(k)}}{\partial x_i} + p^{(k)} + G^{(k)} - \varepsilon \quad (11)$$

Where

$$P^{(k)} = -\overline{u'_i u'_j} \frac{\partial u_i}{\partial x_j} \quad (12)$$

is the turbulence dynamic energy development term due to mean bending and

$$G^{(k)} = \overline{u'_i f'_i} \quad (13)$$

is the turbulence dynamic energy development term due to volume force and

$$\varepsilon = \nu \left(\frac{\partial u'_i}{\partial x_j} \right)^2 \quad (14)$$

is the disappearance of turbulence dynamic energy and

$$d_i^{(k)} = \nu \frac{\partial k}{\partial x_i} \frac{\overline{p' u'_i}}{\rho} - \frac{1}{2} \overline{u'_j u'_j u'_i} \quad (15)$$

is used to obtain turbulence dynamic energy diffusion (FLUENT, 1998).

Numerical Solution

In this work, in order to develop the flow field network, a structured network was used which is an organized structure. Since the type and the density of the mesh influence the results and the timing of the computations, it is required that the precision and the timing be treated carefully to be within the reasonable limits. Hence, the arrangement and the density of the network were studied. In order to precisely develop a turbulent flow field using survival equation so that the details are covered, a computational network with smaller elements than those of flow eddies was used. It means each eddy was divided into several smaller elements.

A 3m×2m×2.8m room was used in this study as the reference geometry (Figure 1). The vertical width of the vertical geometry (distance between the glass and the wall) was 0.15 m, heights of upper, lower holes and wall thickness were respectively 0.28m.

Research Article

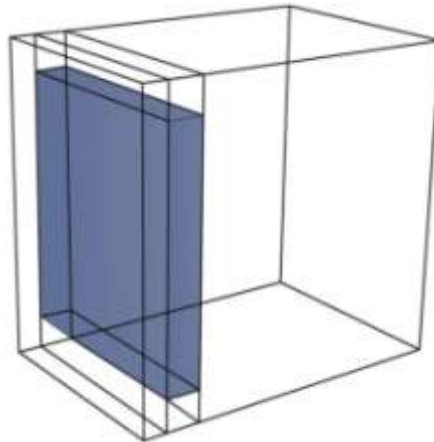


Figure 1: Three-dimensional view of the room with Trombe wall

Nusselt number was selected as a measure to determine the number of cells in the room since it is one of the influential parameters in heat movement. Before that, the satisfaction of the survival equation and obtaining of y^+ was ensured. Hence, it was decided to a finer grid at the air inflow and outflow gates, near walls and in areas where speed gradient was supposed to change quickly. To ensure the independence of results of solving flow equation from the developed network, seven grids with different densities were compared and the resulting Nusselt numbers were represented on the behind and front heat surface with Nu_1 and Nu_2 . The basis for obtaining an independent response from grid is increasing the number of cells until Nusselt number is minimized. In order to save time while solving the problem, the grid with minimum number of cells is selected as the optimum grid (Figure 2). Since from 482724 cells onwards the curve shows a down sloping trend and Nusselt number variations between 610400 and 770400 cells are negligible, therefore 610400 cells were used for the gridding purpose.

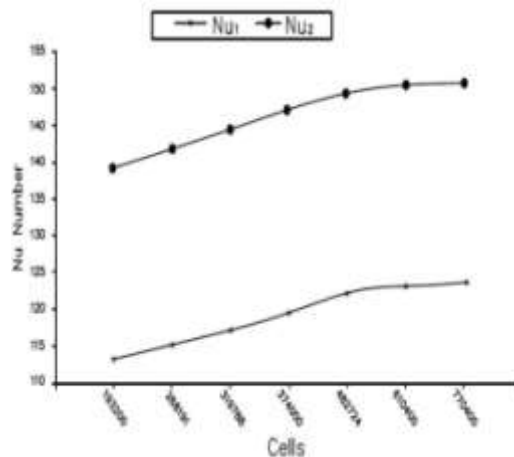


Figure 2: The mean of Nusselt number against cells

Numerical Solution Based on Geometry with Specific Boundary Conditions

All the results of the present study were obtained by first order discrete construction. Also, simple momentum was used to couple continuity and momentum equations. In order to determine the weather conditions, a winter day (13:00 of Jan 5th) in the city of Ahwaz was selected as the reference time. The constants of the weather conditions and other related conditions used in this work are presented in Table (3). Heat transfer is considered for the adjacent walls, roof, floor, and window pane.

Research Article

Table 3: Conditions

Description	Value
Temperature environment	15 °C
Air Prantel	0.71
Air density	1.225 kg/m ³
Specific heat of air	1006.43 j/kg-k
Air thermal conductivity	0.0242 w/m-k
Air viscosity	1.7894 kg/m-s
Coefficient of thermal expansion of air	0.00343 1/k
Masonry wall density	2400 kg/m ³
Specific heat masonry wall	880 j/kg-k
Masonry wall thermal conductivity	1.7 w/m-k
Density glass	2520 kg/m ³
Specific heat of glass	840 j/kg-k
Glass thermal conductivity	0.96 w/m-k
Direct solar radiation intensity	800 w/m ²
Intensity of solar radiation scattered	75 w/m ²
Longitude	48.49 deg
Latitude	31.24 deg
The time difference with GMT	+3.5 GMT
Black wall absorption coefficient	0/9
Glass absorption coefficient	0.1
Glass cross coefficient	0.8

Solar load along with its effects were used in this paper (Ching and Shenq, 1998). By defining solar parameter for solar load, it is required to determine the necessary boundary conditions. Glass was defined as a half-transparent wall and other walls were chosen as dark walls. The dark wall absorption coefficient and that of glass are given in Table 3.

Obtaining Optimal Geometry of Trombe Wall Air Channels to Maximize Heat Transfer

In order to obtain the optimal geometry for Trombe wall channels, three-dimensional simulations were performed and Rayleigh numbers of 10^7 to 10^{10} were obtained for laminar and turbulent flows. Also, the average Nusselt number is for the front surface of the wall. It should be noted that the three dimensions have been considered unchanged under all circumstances.

The ratio of vertical channel width to the height of the room was considered as B/H ; and the ratio of upper and lower vents and wall thickness to vertical channel height were respective considered as C_1/H , C_2/H and E/H . The details are given in Figure 3.

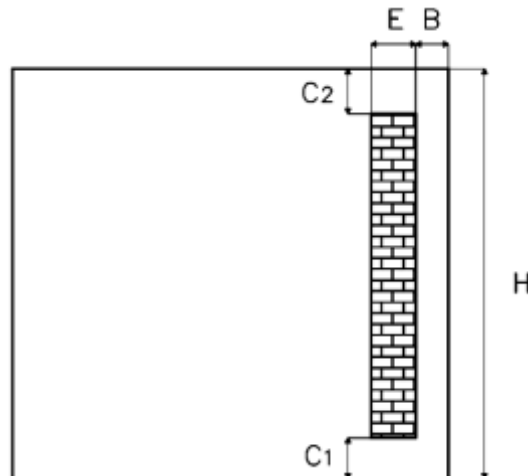


Figure 3: Details of the side view of the room

Research Article

Distance between the Wall and the Glass

The mean Nusselt values were obtained within Rayleigh numbers for $0.084 < B < 0.392$. Other geometrical values were considered unchanged. The resulting values of simulations for non-dimensional view B/H compared to the number of mean Nusselt are shown in Figure 4. Any of the set of points was obtained for a given Rayleigh value for different ratios of B/H. There is a B/H ratio for a given Rayleigh value in which Nusselt number is the maximum. This ratio is called $(B/H)_{opt}$. The results indicate that as the Rayleigh number increases, optimal B/H decreases. In B/H values lower than $(B/H)_{opt}$, this great decrease is due to the heat transfer. When the B/H value is small, the temperature of fluid flow core will increase and be close to the temperature of the wall. Hence, in design, B/H values smaller than $(B/H)_{opt}$ are not appropriate compared to larger B/H. Also, the larger the Rayleigh number is, the more sensitive it is against the B/H variations.

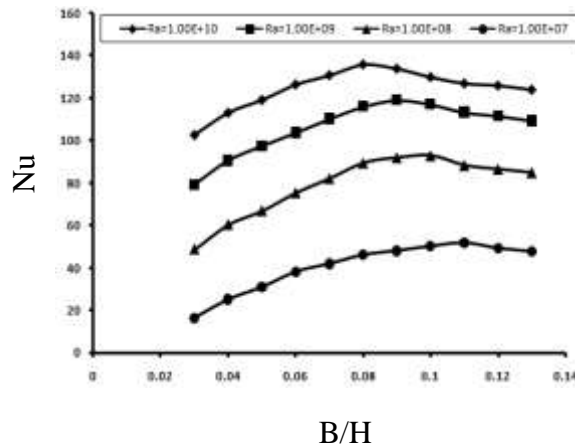


Figure 4: Average Nusselt number versus aspect ratio B/H, for $10^7 < Ra < 10^{10}$, $C_1/H=C_2/H=E/H=0.1$.

Due to the fact that the Rayleigh number is 10^{10} , the optimal B/H ratio is obtained as 0.08.

Bottom Horizontal Channels

The mean Nusselt values were obtained within Rayleigh numbers for $0.084 < C_1 < 0.392$. Other geometrical values were considered unchanged. The resulting values of simulations for non-dimensional view C_1/H compared to mean Nusselt number are given in Figure 5. The curve also indicates that as the Rayleigh number increases, optimal C_1/H decreases. Due to the fact that the Rayleigh number is 10^{10} , the optimal C_1/H ratio is obtained as 0.1.

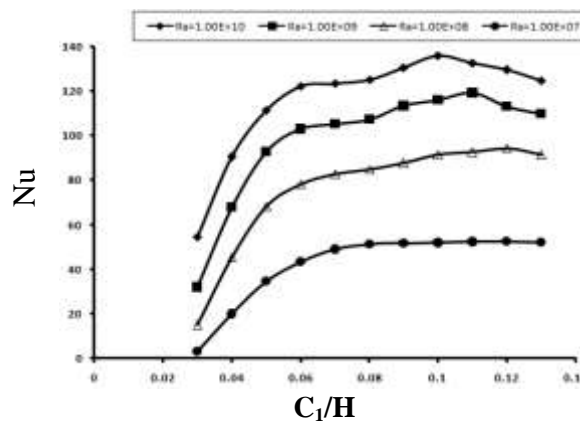


Figure 5: Average Nusselt number versus aspect ratio C_1/H , for $10^7 < Ra < 10^{10}$, $C_2/H=E/H=0.1$, values of B/H results from the Figure (4).

Research Article

Upside Horizontal Channels

The mean Nusselt values were obtained within Rayleigh numbers for $0.084 < C_2 < 0.392$. Other geometrical values were considered unchanged. The resulting values of simulations for non-dimensional view C_2/H compared to the number of mean Nusselt are displayed in Figure 6. The curve also designates that as the Rayleigh number increases, optimal C_2/H decreases. Due to the fact that the Rayleigh number is 10^{10} , the optimal C_2/H ratio is obtained as 0.11.

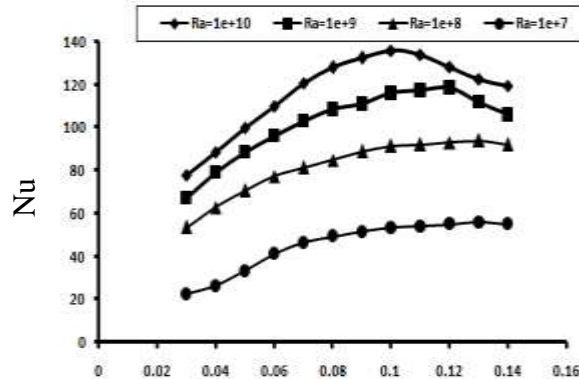


Figure 6: Average Nusselt number versus aspect ratio C_2/H , for $10^7 < Ra < 10^{10}$, 0.1, and values B/H and C_1/H are results from the Figure 4 and 5.

The variations of Nusselt number with Rayleigh values showed that bottom channels affect the heat transfer more than the upper channels.

Wall Thickness

As for the previous cases, simulations were made for $0.084 < E < 0.392$ thicknesses. Other geometrical values were considered unchanged. The resulting values of simulations for non-dimensional ratio of E/H compared to the number of mean Nusselt are shown in Figure 7. This figure also shows that as the Rayleigh number increases, optimal E/H decreases. Due to the fact that the Rayleigh number is 10^{10} , the optimal E/H ratio is obtained as 0.11.

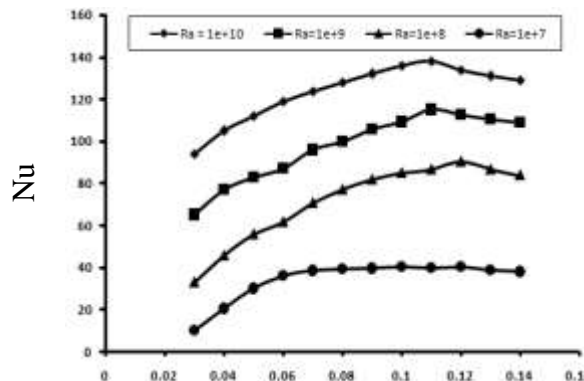


Figure 7- Average Nusselt number versus aspect ratio E/H , for $10^7 < Ra < 10^{10}$, Values of B/H , C_1/H and C_2/H are results from the Figure (4), (5) and (6).

Optimized Geometry: Results

As the fluid moves upward in the vertical channel, the air is expanded and its density decreases. Free movement occurs when a volumetric force resulting from gravitational field acts upon a fluid with density slope. The net effect will be the development of a buoyancy force which causes free movement. This buoyancy is caused by simultaneous existence of fluid density slope and the volumetric force proportionate to fluid density.

Research Article

At the channel, the fluid temperature is lower than the temperature of wall and glass. Hence the portion of fluid close to wall has a lower density than that further from the wall. And the buoyancy forces develop a free movement boundary condition in which the heated fluid moves upward carrying fluid in the steady area. Warm air enters the room from the upper channel while cold air enters from the lower channel.

The temperatures of dark wall and glass are presented in Table 4. Obviously, the temperature of glass surface is lower than that of wall; and the temperature of the front wall is lower than that of the back wall.

Table 4: Temperature the glass and wall

Temperature	Glass ($^{\circ}C$)	Front surface heat wall ($^{\circ}C$)	Dorsal surface heat wall ($^{\circ}C$)
Mean temperature	27	38	34
Maximum temperature	28	50	47

Temperature distribution over vertical and horizontal planes within the room is displayed in Figure 8 and 9.

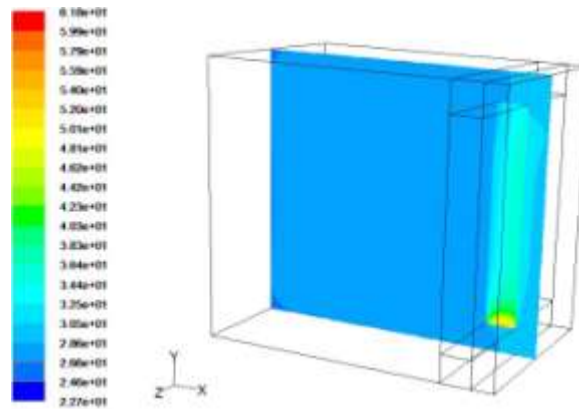


Figure 8: Temperature distribution in the vertical plate

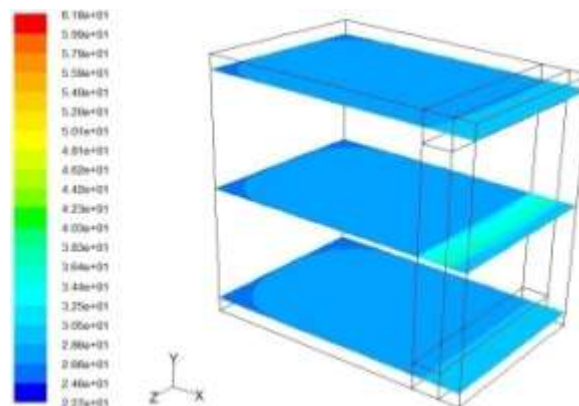


Figure 9: Temperature distribution in the horizontal plates

A review of Figure 10 and 11 indicates that as the temperature increases, Rayleigh number increases and consequently Archimedes forces and speed increase. The resulting speed distribution does not resemble the speed distribution in boundary condition movement as at $y=0$ and $y \rightarrow \infty$, speed closes to zero.

Research Article

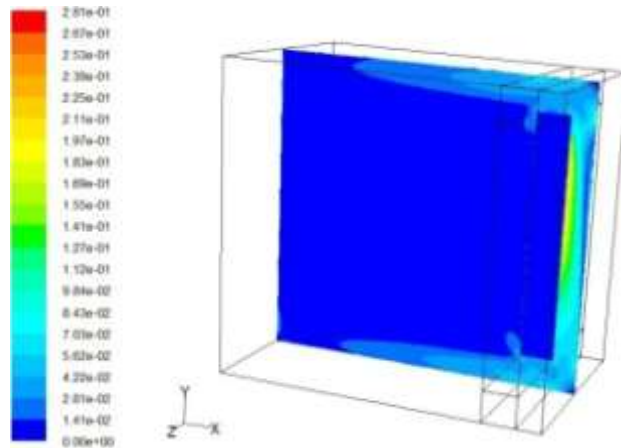


Figure 10: Velocity distribution in the vertical plate

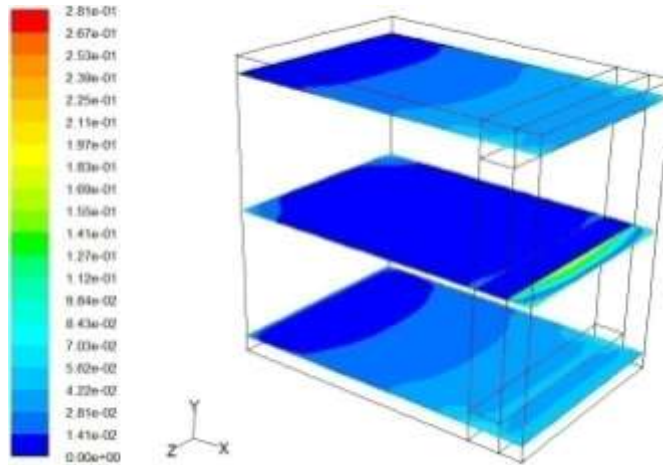


Figure 11: Velocity distribution in the horizontal plates

Considering the above figures, due to air expansion at the channel outlet and air suction at the channel entrance, the speed rises. Figure 12 shows the flow lines while Figure 13 presents speed distribution.

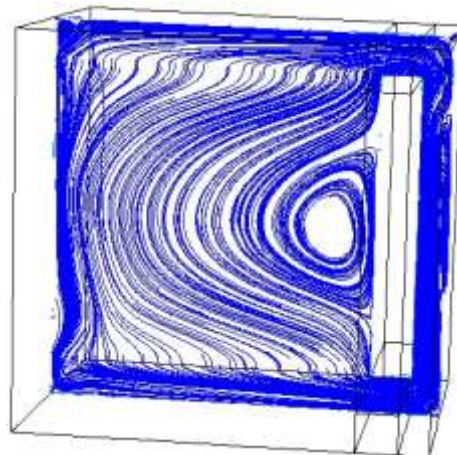


Figure 12: Stream lines ($Ra=10^{10}$)

Research Article

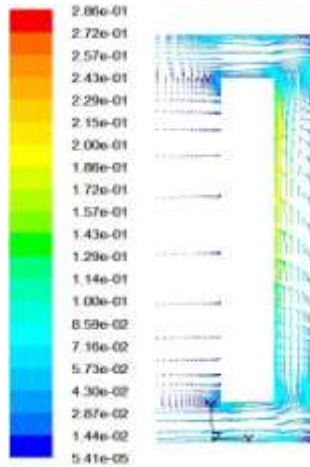


Figure 13: Showing the speed vectors ($Ra=10^{10}$)

As indicated in Figure 12, one can conclude that an eddy is formed behind the heated wall. Figure 8 also indicates that the air channel edges reduce the air velocity.

Results of Optimized Geometry by Removing Air Channel Sharp Edges

In order to solve the above-mentioned problems and improve heat transfer, the removing of air channel sharp edges is discussed in this section (see Figure 14).

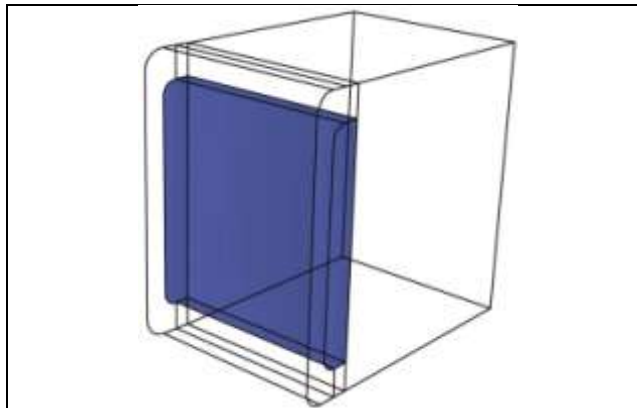


Figure 14: Three-dimensional view of the room with curved corners Trombe wall

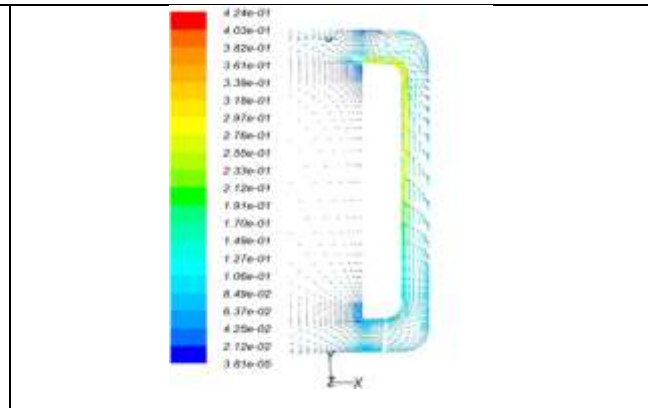


Figure 15: Velocity vector display for the channel with curved corners

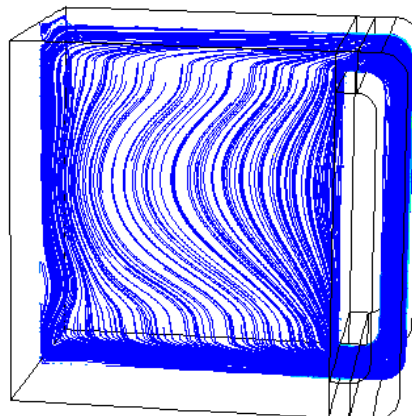


Figure 16: Show stream lines for the curved channel

Research Article

The results of simulation show that flow speed is considerably increased (see Figure 15). Also, the flow lines (Figure 16) indicate that no traces of the eddy can be found behind the wall. In other words, disappearance of eddy can be seen as one of the speed rise factors.

Comparing the average Nusselt values for channels with round edges and those with sharp edges indicates that it has increased for 10 percent hence one can conclude that the amount of transferred heat has increased and room temperature has risen.

Conclusions

The general conclusions can be drawn as follows:

1. Considering the turbulent current and existence of buoyancy forces, in order to model the disturbance, two-equation $k-\varepsilon$ shear stress models were used for determining the free movement flow. Then after modeling and comparing the results of numerical models with experimental models, Reynolds shear stress model was selected.
2. After obtaining optimized geometry for channels it was indicated that since the passing air from upper channel is more heated with higher speed and energy, the effect of lower channel variations on heat transfer is higher than the upper ones. Also, it was observed that the optimized value of all geometric parameters including distance of thermal wall from glass, wall thickness and the area of upper and lower vents decrease as Rayleigh number decreases. So it can be said that Rayleigh is a free convection heat transfer engine. With increasing Rayleigh this engine becomes stronger and will have more ability for mass transfer.
3. By removing sharp edges of air channels it became obvious that the mean Nusselt number has increased considerably as compared to those still with sharp edges. Hence, heat transfer increased and room temperature rose. Also, no eddies were formed behind the heat wall.

Designation

- B Wall-to-wall spacing of the vertical channel (m) (Figure 3)
 C_1, C_2 Bottom and top opening heights, respectively (Figure 3) (m)
 c_p Specific heat at constant pressure ($\text{J kg}^{-1}\text{K}^{-1}$)
E Thickness of the Trombe Wall (Figure 1) (m)
g Gravitational acceleration (m^{-2})
Gr Grashof number
h Local heat transfer coefficient ($\text{W m}^{-2}\text{K}^{-1}$)
k Turbulent kinetic energy (m^2s^{-2})
H Height of the wall (Figure 3) (m)
L Length (m)
Nu Nusselt number
P Average reduced pressure (N m^{-2})
Pr Prandtl number
q Wall heat flux (W m^{-2})
Ra Rayleigh number
T Temperatures (c)
 U_j, u_j Average and turbulent components of velocity, respectively (m s^{-1})
x, y, z Cartesian coordinates in the three-dimensional directions (m)

Greek Symbols

- β Coefficient of thermal expansion (K^{-1})
 μ Viscosity ($\text{kg m}^{-1}\text{s}^{-1}$)
 ρ Density (kg m^{-3})
 ν Kinematic viscosity (m^2s^{-1})
 ω Specific dissipation rate of k (or turbulent frequency) (s^{-1})
 ε Rate of dissipation of kinetic energy
 α Thermal diffusivity (m^2s)

Research Article

Subscripts

- 1 Outer wall (corresponding to glazing)
- 2 Inner wall (corresponding to masonry wall)
- max Maximum
- opt Optimum
- w Wall
- Superscript
- Averaged value

REFERENCES

- Akbari H and Borgers TR (1979).** Free convective laminar flow within the Trombe wall channel. *Solar Energy* **22** 165-174.
- Chen B and Zhuang Z (2006).** Experimental investigation of natural convection in Trombe wall system, *Envelope Technologies for Building Energy Efficiency* **2** 1-3.
- Ching GC and Shenq YJ (1998).** *Fundamentals of Turbulence Modeling* (Taylor & Francis).
- Dehghani AR and Aghanajafi S (2007).** *Solar Radiant Heat Transfer and its Application in Building* (Publications KhwajaNasirToosi University of Technology).
- Fedorov AG and Viskanta R (1997).** Turbulent natural convection heat transfer in an asymmetrically heated, vertical parallel-plate channel. *International Journal of Heat and Mass Transfer* **40** 3849-3860.
- FLUENT 6 (1998).** *FLUENTS User's Guide*, (Incorporated) **11** 78-82.
- FLUENT 6 (1998).** *FLUENTS User's Guide*, (Incorporated) **13** 108-125.
- Galal MJ and Sajda SF (2006).** Simulation of trombe wall in Baghdad atmosphere. *Solar Energy* **26** 66-71.
- Kaiser A, Zamora B and Viedma A (2004).** Correlation for Nusselt number in natural convection in vertical convergent channels at uniform wall temperature by a numerical investigation. *International Journal of Heat and Fluid Flow* **25** 671-682.
- Peng S and Davison L (1999).** Computation of turbulent buoyant flows in enclosures with low-Reynolds number k-omega models. *International Journal of Heat and Fluid Flow* **20** 172-184.
- Smolec W and Thomas A (1993).** Theoretical and experimental investigating of heat transfer in a Trombe wall. *Energy Convers* **34** 385-400.
- Versteeg HK and Malalasekera W (1995).** *An Introduction to Computational Fluid Dynamics* (Loughborough).